

AC losses of Rutherford MgB_2 cables made by powder-in-tube and internal magnesium diffusion processes

J Kováč[✉], M Kulich, L Kopera and P Kováč[✉]

Institute of Electrical Engineering, Slovak Academy of Sciences, Dúbravská cesta 9, 841 04 Bratislava, Slovakia

E-mail: jan.kovac@savba.sk

Received 19 July 2018, revised 8 October 2018

Accepted for publication 11 October 2018

Published 5 November 2018



Abstract

Magnetization losses of Rutherford MgB_2 cables of different sheath materials (Cu, CuNi and $\text{Al} + \text{Al}_2\text{O}_3$) made by powder-in-tube and internal magnesium diffusion processes were studied experimentally. Short cable samples consisting of 12 strands were measured in the temperature range from 18 K up to 40 K, external fields up to 70 mT and frequencies 72 Hz and 144 Hz. The effects of inter-strand resistance by soldering and external field orientation (perpendicular and parallel) were also tested. The impact of eddy current losses in the sheath material was determined by the loss measurement in cable samples without MgB_2 . It was found that very high eddy current losses of Cu sheathed strands overlap the hysteresis loss. The lowest AC losses at 20 K were measured for a Rutherford MgB_2 cable with an $\text{Al} + \text{Al}_2\text{O}_3$ sheath, which makes it attractive for applications where low loss and also low coil mass are required (e.g. wind turbines or airborne engines).

Keywords: MgB_2 cables, AC losses, eddy currents, Rutherford cables

(Some figures may appear in colour only in the online journal)

Introduction

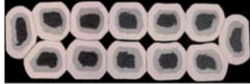
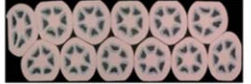

Rutherford cable has played a key role in establishing NbTi accelerator magnet technology. Superconducting dipoles and quadrupoles based on this cable design were successfully used in Tevatron, HERA and the Large Hadron Collider, and new generation magnets using NbTi and Nb_3Sn Rutherford cables are also still developed [1–3]. Properties of Rutherford cables based on Nb_3Al and Bi-2212 superconductors were also reported [4, 5]. The advantages of a lightweight MgB_2 superconductor for a 10 MW wind generator, as well as the development of stator windings for a fully superconducting motor with MgB_2 wires were described [6, 7]. Cables made with appropriate transposition length allow a substantial reduction in AC losses in comparison to monolithic wires. When a local normal region is generated in a strand of cable, the current in the strand is shared into other strands. Consequently, stability problems caused by current sharing between strands may arise. The current sharing occurs in advance of propagation of a

normal state and the duration of the current sharing depends on the current margin of the cables [8]. While hysteresis loss due to screening currents induced into superconducting cores can be minimized by lowering the filament size, the coupling current losses can be reduced effectively by the transposition and by increased inter-strands (or crossover) resistance. It was already shown that decoupling by twisting of the filaments in filamentary wires has practical limits due to considerable degradation of the transport current properties. On the other hand, cabling of not-reacted strands does not cause degradation of transport currents, but reduces AC losses effectively [9]. Recently, a few Rutherford MgB_2 cables assembled from strands manufactured by powder-in-tube (PIT) and also by internal magnesium diffusion (IMD) processes have been successfully manufactured and characterized at low temperatures [10–13]. Rutherford MgB_2 cables are not suitable for high field accelerator magnets, but are more promising for low field applications at temperatures around 20 K where minimized AC losses are also required (e.g. for wind turbines or for



Figure 1. The outer surface of the examined Rutherford MgB_2 cable IMD-Al.

Table 1. Basic properties of Rutherford MgB_2 cables made of 12 strands.

Sample	PIT-CuNi	PIT-Cu	IMD-Al
Length [mm]	67	66	65
J_e (4T, 20K) [Acm^{-2}]	560/1120	297/594	665/1330
Cross-section			
Out. size [mm]	2.55 x 0.79	2.55 x 0.73	2.90 x 0.87
Sc. area [mm^2]	0.329	0.230	0.196
MgB_2 area [%] / doping	19.8 / no	12.7 / C	9.6 / no
Sheath material	Cu_{10}Ni	Cu	$\text{Al}+1.5\%\text{Al}_2\text{O}_3$
Diffusion barrier	Nb	Nb	Ta
Heat treatment [$^\circ\text{C}/\text{min}$]	650/20	650/40	630/10

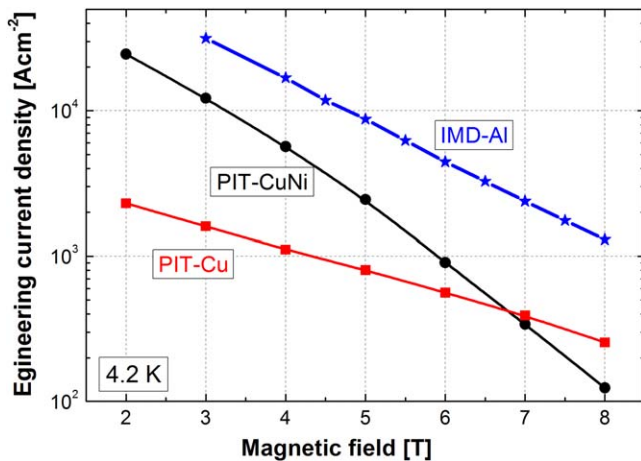


Figure 2. A comparison of engineering current densities of Rutherford MgB_2 cables at 4.2 K.

superconducting motors of high power density in aircraft). Rutherford cable offers reduced AC losses and also lowered bending diameter, which is important especially for multi-pole race-track windings made of already reacted cable [10].

The aim of this work is to study and compare the AC losses in Rutherford type MgB_2 cables assembled of strands having different metallic sheaths and manufactured by PIT and IMD processes.

Experimental details

Three types of Rutherford MgB_2 cables assembled from 12 wires with different metallic sheaths made by PIT [10] and IMD processes [11] were selected for AC loss measurements at low temperatures. The used cabling system consists of a

stranding machine with 12 back-twist supply spools, a powered forming roller, caterpillar, and take-up reeling machine [10]. All cabling modules are synchronized to allow continuous control of the cabling speed versus transposition length. All wires are helically stranded around the mandrel fixed in the central axis, which is gradually changing shape from circular into a flat trailing end. The shaped strands enter from the trailing end of the mandrel into a driven roller head where compacting and final rectangular shaping of the cable is performed. During the cabling process the wires experience some plastic deformations that modify the geometrical dimensions of the sub-elements, see cross-sections in table 1. The main properties of examined cable samples, named according to the manufacturing process used and the metallic sheath as PIT-Cu, PIT-CuNi and IMD-Al, are summarized in table 1. Two cables (PIT-Cu, PIT-CuNi) were made by an *in situ* process using C-doped six-filament wires and undoped single-core wires of 0.39 mm in diameter produced by HyperTech [10]. The transposition length of both cables was 20 mm, the width was 2.55 mm and the final thickness was 0.73 mm and 0.79 mm, respectively. Single-core not-doped MgB_2 wires made by IMD processes of diameter 0.465 mm with a Ta barrier and an $\text{Al} + \text{Al}_2\text{O}_3$ outer sheath were used for cable IMD-Al [11]. The transposition length of the IMD-Al cable was $L_t = 20$ mm, with width 2.9 mm and the final thickness 0.87 mm, see figure 1. Table 1 shows the basic parameters and cross-sections of the examined cables. To compare the critical current of all cables and individual strands, a standard DC current transport measurement with a $1 \mu\text{Vcm}^{-1}$ criterion was used. Critical currents of individual strands between temperatures 4.2 K and 20 K were obtained by the AC transport option in the PPMS system by Quantum Design, where the current amplitude is limited to $I < 2$ A. $R(T)$ dependencies of the cable samples were measured by a

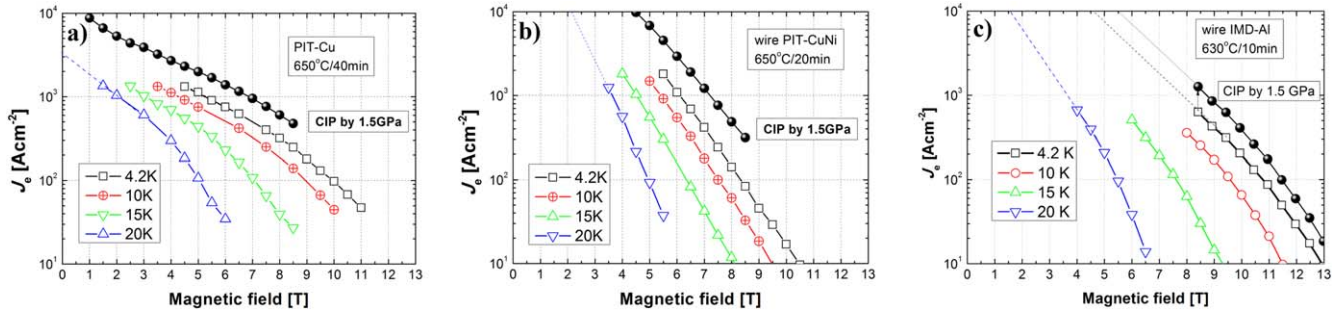


Figure 3. Engineering current densities of as-drawn and heat-treated strands used for PIT-Cu (a), PIT-CuNi (b) and IMD-Al (c) cables. Filled circles in each figure present the J_e values of wires pressed prior to final annealing by 1.5 GPa and measured only at 4.2 K.

four-probe method to estimate the differences in critical temperatures and in normal state resistances. AC losses of short cable samples were measured by the system based on the calibration free method with small modifications allowing a higher sensitivity of measurements [14]. The applied magnet system consists of two identical race-track magnets connected in series generating an external magnetic field oriented perpendicular and/or parallel to the plane of the cable sample at a temperature range of 18 K to 40 K. For elimination of the magnet's self losses by eddy currents these windings are made from cable made of thin copper insulated wires. Another winding is placed inside each magnet and these two coils are connected in anti-series. The first one serves as a pick-up coil and the second one as a compensation coil [15]. For the determination of AC loss a standard lock-in technique is used. AC field amplitudes from 7×10^{-4} T up to 7×10^{-1} T in root mean square and two frequencies, 72 Hz and 144 Hz, were applied for cable samples of length ≈ 66 mm [15]. AC losses Q (J m^{-3}) were estimated for the whole cable volume and plotted versus the temperature or magnetic field. For the estimation of only eddy current loss generated in metallic sheaths, cable samples annealed at low temperature $450^\circ\text{C}/30$ min (without the superconducting MgB_2 phase) were measured between 20 K and 60 K.

Results and discussion

Figure 2 shows engineering current densities versus the external field of the three examined Rutherford MgB_2 cables measured at 4.2 K. Apparent are the differences in $J_e(B)$ resulting mainly from different filament size, the manufacturing process used and also C-doping into MgB_2 . Although the IMD-Al cable has the lowest content of the MgB_2 phase (9.6%), it has the highest engineering current densities between 2 and 8 T. In addition, the IMD-Al shows a less steep decrease in the critical current with the external field in comparison to PIT-CuNi, which can be attributed to the well-connected and fine grain MgB_2 structure obtained by the IMD process [16].

Figure 3 shows in-field engineering current densities of individual cable's strands after drawing and annealing at the conditions identical to those for the assembled cables.

$J_e(B, 4.2 \text{ K})$ dependencies (plotted by the filled circles) exhibit improvement of the current density by densification of the powder inside the strands by cold isostatic pressing with 1.5 GPa prior to annealing, which has (according to our experience) a similar effect to the densification of strands in Rutherford cable by two-axial rolling [11]. Therefore, table 1 shows two values of $J_e(4 \text{ T}, 20 \text{ K})$ for each cable where the lower values are determined from the measured characteristics in figure 2, and the higher (doubled) values are J_e estimated for the cables subjected to additional densification by rolling or pressing. The degradation by cabling can be obtained by the comparison of J_e at 4.2 K in cables (figure 2) and in corresponding wires (figure 3). Figure 2 shows $J_e = 10^3 \text{ A cm}^{-2}$ measured at an external field of 6 T for PIT-CuNi, at 4.25 T for PIT-Cu and at 8.5 T for IMD-Al. The same J_e values were reached at 6.0/7.3 T (as-drawn/pressed) for PIT-Cu wire, at 5.2/7.0 T for PIT-CuNi wire and at 7.8/8.8 T for IMD-Al wire. This indicates that slight degradation occurred in the PIT-CuNi cable having the same J_e as in the as-drawn strand. Large degradation of the current density is evident for PIT-Cu cable with 10^3 A cm^{-2} measured at 4.25 T, while PIT-Cu wire reaches it at 5.2 T in the as-drawn state and at 7 T after cold isostatic pressing by 1.5 GPa. The IMD-Al cable with 10^3 A cm^{-2} at 8.5 T shows the minimal degradation where nearly the same J_e was measured at fields 7.8/8.8 T in wires used for cabling. While J_e values at 20 K are quite similar for the PIT-CuNi and IMD-Al strands (10^4 A cm^{-2} at 1.5–2 T), J_e lowered by one order of magnitude (10^3 A cm^{-2}) was measured for the C-doped PIT-Cu strand at the same field and temperature. Extrapolation of J_e into very low field regions (e.g. 50–70 mT, where AC losses were measured) may lead to relative high inaccuracy and, therefore, is omitted.

Figure 4 shows the temperature dependence of AC losses for the PIT-Cu cable with the superconducting MgB_2 phase in comparison to not-superconducting, not-annealed (AD—as-drawn) and low temperature annealed ($450^\circ\text{C}/30$ min) cable samples. While eddy current losses in both not-superconducting cables are comparable at ~ 60 K, much higher losses are observed for the sample annealed at $450^\circ\text{C}/30$ min in the temperature region of 20–40 K. This increase is due to improved conductivity of the Cu used in the PIT-Cu cable after annealing. The insert in figure 4 compares the measured

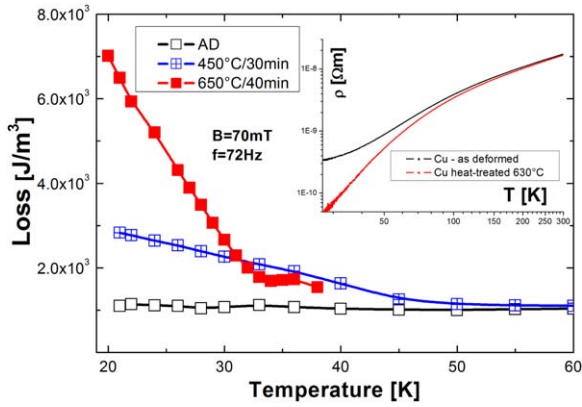


Figure 4. AC losses in as-deformed (AD) PIT-Cu cable (without MgB_2) and annealed cables at 450 °C (without MgB_2) and 650 °C (with MgB_2). The insert shows $R(T)$ dependencies for as-deformed and heat-treated Cu at 630 °C.

$\rho(T)$ characteristics of hard drawn and soft annealed Cu at 630 °C used for the sheath of the cable strands. One can see an apparent decrease in the $\rho(T)$ characteristic for the annealed Cu, especially at low temperatures below 50 K. An apparent increase in AC loss is observed below 30 K in PIT-Cu cable annealed at 650 °C/40 min in comparison to 450 °C/30 min, which can be ascribed to the effect of the superconductor's diamagnetism. In addition, large coupling current losses inside the six-filament not-twisted Cu sheathed strands can be expected. In cable containing MgB_2 the magnetic field is expelled out of superconducting filaments, which causes a local increase in the magnetic field in the copper sheath and subsequent higher eddy current losses in comparison to cable without a MgB_2 phase.

To see only the impact of eddy currents in different sheath materials, magnetization losses in examined cable samples without MgB_2 were measured. Figure 5 compares the eddy current losses of cables annealed at 450 °C/30 min, which are comparably low for the Al + Al_2O_3 sheath (996 J m^{-3} at 20 K) and Cu_{10}Ni sheath (969 J m^{-3} at 20 K), but considerably higher for the Cu sheathed cable, especially at temperatures below 40 K (2830 J m^{-3} at 20 K). High eddy current losses in PIT-Cu cable are clearly connected with low electrical resistivity of the annealed Cu sheath, see the insert in figure 4.

Figure 6 shows the temperature dependencies of AC losses in all of the cables, where figure 6(a) presents the total measured AC losses and figure 6(b) shows losses without eddy currents (only hysteresis and coupling losses together). For the samples PIT-CuNi and IMD-Al the losses have mainly hysteresis behavior. Taking into account Bean's model of critical state [17] the induced screening currents are flowing in a layer near to the surface and the thickness of this layer depends on critical current density. Because the critical current density is higher at lower temperature, the thickness of the layer occupied by the screening currents is decreasing with temperature. The magnetization is given as the magnetic moment divided by the volume of the zone occupied by the

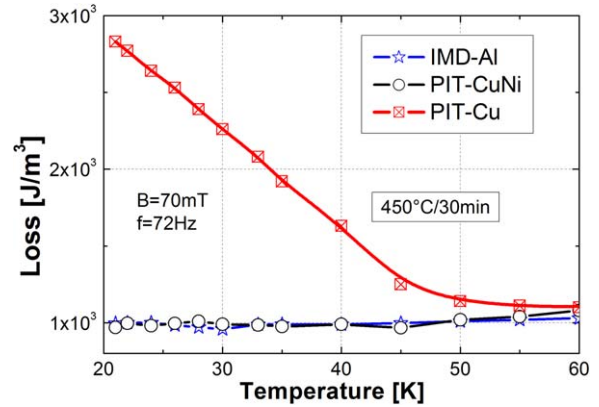


Figure 5. Eddy current losses of not-superconducting cable samples (annealed at 450 °C/30 min) measured at a field of 70 mT and frequency 72 Hz.

screening currents, and, therefore, taking into account formula (2), hysteresis loss is decreasing with temperature below the loss maximum.

Contribution of the eddy current loss component has been subtracted on the basis of data shown by figure 5. By comparison of the curves in figures 6(a) and (b) one can clearly see the effect of the eddy current loss component in all cables. The largest contribution of the eddy current loss is evident in the PIT-Cu cable due to the highly conductive Cu sheath, which agrees with the theoretical assumption. The dissipation Q —lost per cycle and per volume unit due to eddy currents—can be expressed by the formula:

$$\frac{Q}{V} = \frac{\pi^2 B_p^2 d^2 f}{6k\rho} \quad (1)$$

where B_p is the peak magnetic field and f its frequency, d is the diameter of the wire and ρ is the resistivity of the material [18]. Equation (1) shows that the loss will be greater for lower sheath resistivity. The constant k represents the factor of wire geometry and is equal to 2 for a thin wire.

The lowest total AC losses for the IMD-Al cable with the smallest eddy current component were measured at 20 K, see figure 6(a). Figure 6(b) shows no hysteresis losses in the PIT-Cu cable after extracting eddy current components. No local maximum has been found for the PIT-Cu cable at the given temperature range because of the high shielding effect of eddy currents and much lower current densities (by \approx one order of magnitude) in comparison to IMD-Al and PIT-CuNi, see figure 3. Comparable losses are observed for IMD-Al and PIT-CuNi at temperatures around 20 K due to low hysteresis loss and effective decoupling of individual strands. As one can see, the AC loss maximum is shifted to a lower temperature for IMD-Al. The loss maxima at 31 K and 34 K are measured for the IMD-Al and PIT-CuNi cable, respectively. This is due to the critical temperatures of these cables differing by ~ 3 K, see figure 7. The middle of the $R(T)$ transitions was used for the estimation of critical temperature T_c , which corresponds to 39.1 K for PIT-CuNi, 36.6 K for IMD-Al and only 34.1 K for PIT-Cu due to C-doped MgB_2 . Figure 7 also shows large differences in normal state resistances, which is around two

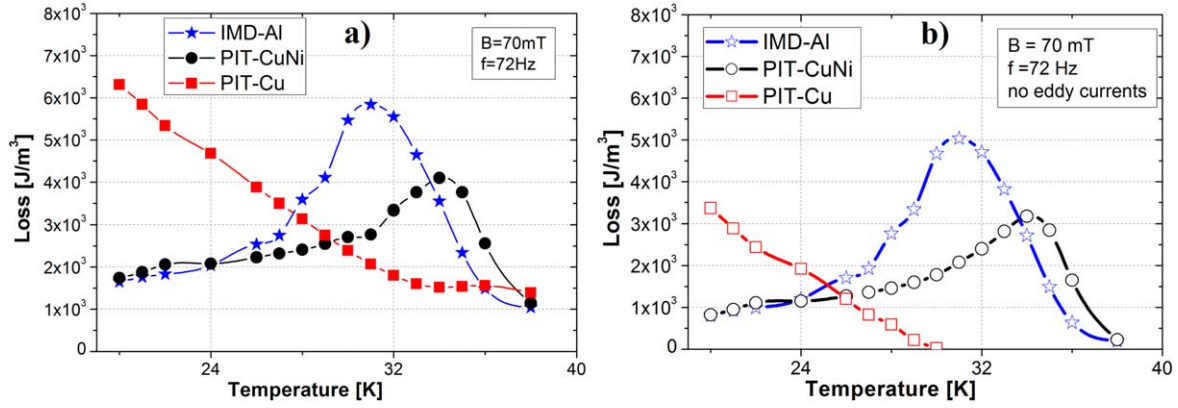


Figure 6. The temperature dependencies of total AC losses in all cables measured at a perpendicular field of 70 mT and frequency 72 Hz (a) and AC losses after subtraction of the eddy current loss component (b).

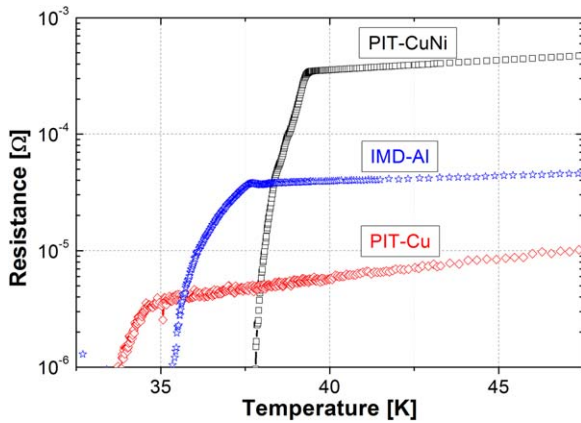


Figure 7. Resistive transitions of cables measured by a four-probe method.

orders of magnitude lower for PIT-Cu in comparison to PIT-CuNi.

In the case of well-insulated strands the total loss should be given as the sum of losses of individual strands, but some connections and shielding also have to be expected in real conditions. Therefore, experiments showing how the losses of Rutherford cable can be affected by inter-strand connections have been performed for IMD-AI cable. Figure 8(a) shows the $Q(T)$ characteristics measured at external field 50 mT and two frequencies 72 Hz (filled stars) and 144 Hz (empty stars) for an IMD-AI cable in a perpendicular magnetic field orientation compared with the same cable which has inter-strand voids filled by CdZn solder. The losses of non-soldered cable dominantly represent the hysteresis behavior with a small impact of eddy currents, discussed above. The loss maximum represents the state, when the superconducting filaments are fully penetrated by the external field. By lowering the temperature, the critical current density increases and the magnetic field is forced out of the superconducting filament because the screening currents are flowing in a thinner layer at the surface of the superconductor. The hysteresis loss is found as the area of the magnetization curve:

$$Q_m = \oint B dM = \oint M dB \quad (2)$$

where Q_m is the magnetic loss per volume of the superconductor (in Joules per field cycle), B is the external magnetic field and M is the magnetization given by the magnetic moment of sample m per volume which depends on the screening current distribution. The magnetic moment can be expressed as $m = \mu_0 AI$, where A is the area of the current loop. Consequently, a higher J_c means a higher hysteresis loss. Hysteresis loss per cycle is not influenced by the duration of the cycle and therefore it had to be frequency independent.

Different behavior is observed in cable with soldered (well coupled) strands, see figure 8(a). As one can see, the total AC losses of soldered cable are apparently increased, especially at low temperatures ($T < 27$ K). Even the losses above the critical temperature (36.6 K) are increased by soldering and are also frequency dependent, see figure 8(a). This can be attributed to two dominant reasons; (i) additional eddy current losses in the added CdZn solder and (ii) increased coupling current losses due to reduced inter-strands resistance. The total losses of soldered cable in the low temperature region remain high, do not show dependence on temperature and the effect of increased frequency is more expressive as for the not-soldered case. These effects can be explained by coupling current losses due to induced currents flowing along the superconducting strands and across the CdZn solder.

As results from equation (2), the loss of cable depends on its magnetization which is given by the magnetic moment. The simulations in figures 9(a) and (b) show the screening currents and field distribution in the cable exposed to a perpendicular magnetic field oriented to the cable's plane with connected (figure 9(a)) and disconnected strands (figure 9(b)), respectively. In the first case the induced screening currents flowing on the surface of the superconducting layer are circulating along each wire. The red region represents the area occupied by critical current density, while the blue region has the same current but an opposite direction. If the wires behave fully insulated then the total magnetic moment of the cable will be the sum of the individual magnetic moments from each wire. On the other hand, figure 9(b) shows the case where the wires are electrically connected at both ends creating a loop. Consequently, in one

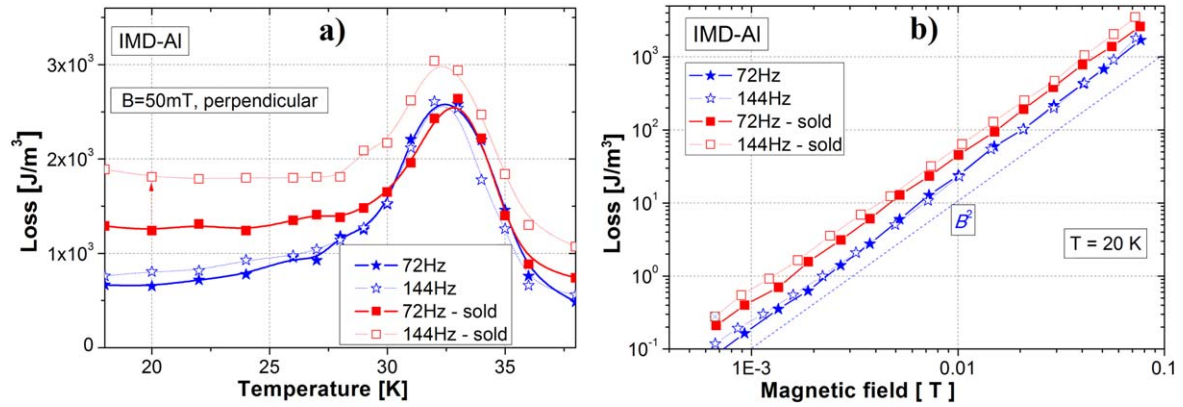


Figure 8. Temperature (a) and the field (b) dependencies of AC losses of IMD-AI cable measured in a perpendicular field, compared with AC losses of the cable penetrated by a CdZn solder.

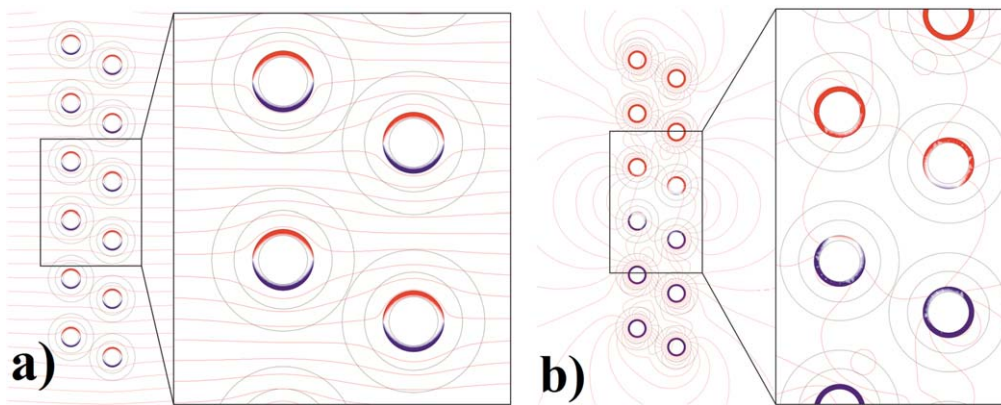


Figure 9. Simulation of superconducting currents and field distribution for the external perpendicular field direction for the cable plane with insulated strands (a) and fully coupled strands (b).

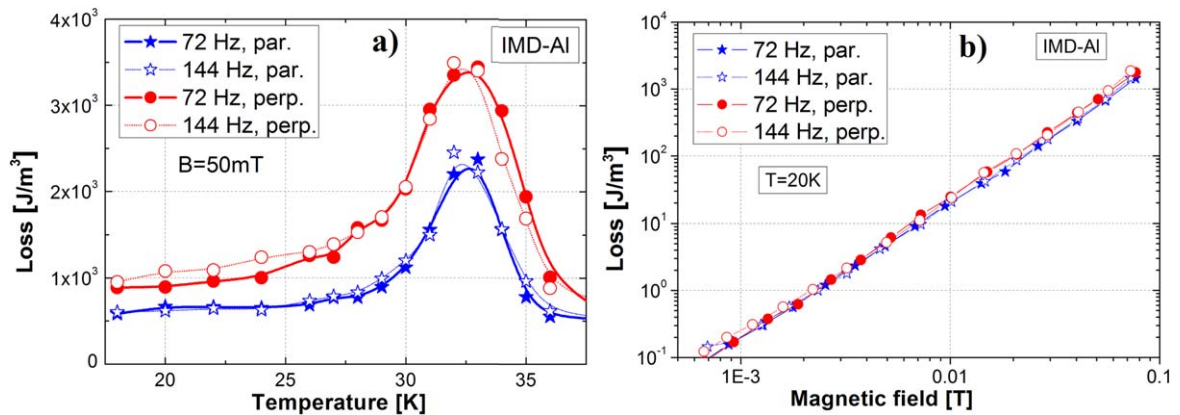


Figure 10. AC losses of IMD-AI cable versus temperature at perpendicular and parallel field orientation of 50 mT and frequencies 72 and 144 Hz (a) and $Q(B)$ dependencies at 20 K (b).

part of the strands the induced current is flowing in one direction (red region), while it flows in the opposite direction in the second part (blue region). Such current distribution creates one resulting magnetic moment, which is larger than the sum of the individual wires' moments. Therefore, coupled wires generate a higher loss in an alternating external magnetic field [18, 19]. Figure 8(b) shows the losses in IMD-AI cable with separated and soldered strands at 20 K versus the external field. As one can see, strand soldering has

increased the losses approximately by two times in the whole range of the external field and they are also increased with frequency.

It should be noted that in the inter-strands resistance of the IMD-AI cable can be additionally increased by anodic oxidation of the strand's surface, which could noticeably reduce the coupling currents.

As already indicated, the shielding effect is a phenomenon, which can noticeably affect a cable's overall losses.

Therefore, AC losses at two orientations of external magnetic field, perpendicular and parallel field were also measured and analyzed.

Figure 10(a) shows the temperature dependencies of losses at 50 mT and at two frequencies 72 Hz and 144 Hz. It is evident that the losses measured over the whole temperature range in parallel orientation are ~ 1.5 times lower in comparison to the perpendicular one. This reflects the effect of different strand shielding. Figure 10(b) shows the $Q(B)$ dependence at 20 K. One can see the identical slopes for both orientations and frequencies $Q(B) \sim B^2$ with only slight dependence on frequency visible for the perpendicular field. Lower losses in the parallel field can be beneficial for possible applications of Rutherford cable in coils where the parallel field is dominant. But, increased losses can be expected at solenoid edges where the perpendicular field direction approaches its maximum.

Conclusion

Magnetization losses of 12-strand Rutherford MgB_2 cables made by PIT and IMD processes were studied. Short cable samples were measured at temperatures ranging from 18 K up to 40 K, external magnetic field up to 70 mT and frequencies 72 Hz and 144 Hz. Total AC losses of Rutherford cables with $\text{Al} + \text{Al}_2\text{O}_3$, CuNi and Cu sheathed wires were compared. Contribution of the eddy current loss in a metallic sheath was quantified by the measurement of AC loss for cable samples in which a MgB_2 phase was not created. It was found that the total AC losses of the IMD cable with an $\text{Al} + \text{Al}_2\text{O}_3$ sheath at 20 K (996 J m^{-3}) were comparable with a Cu_{10}Ni sheathed PIT cable (969 J m^{-3}), but considerably higher for Cu sheathed cable, especially at temperatures below 40 K (2830 J m^{-3} at 20 K). Consequently, high electrically conductive copper sheath is not suitable for use in AC applications. On the other hand, the light $\text{Al} + \text{Al}_2\text{O}_3$ sheathed cable showed high transport properties and also low AC losses, which seems to be promising for real applications.

Soldering of $\text{Al} + \text{Al}_2\text{O}_3$ sheathed cable by CdZn caused additional losses due to more coupled strands and additional eddy currents in the solder layer. Anodic oxidation of the aluminum sheathed strands can be an effective way for further reduction of coupling currents through the increased inter-strands resistance.

The effect of external field orientation has shown higher losses for the field oriented perpendicular to the cable plane, which is explained by different strand shielding. Lower AC losses measured in the parallel field are beneficial for applications of Rutherford cable in coils where the parallel field is dominant. But, increased losses can be expected close to the

flanges of the coils with the field approaching the perpendicular direction.

Acknowledgments

This work was supported by the Slovak Scientific Agency under the project APVV-14-0522 and grant agency VEGA 2/0129/16.

ORCID iDs

J Kováč  <https://orcid.org/0000-0001-9127-9681>

P Kováč  <https://orcid.org/0000-0003-1872-0359>

References

- [1] Barzi E, Andreev N, Boffo C, Borissov E, Elementi L, Del Frate L, Yamada R and Zlobin A V 2004 *Supercond. Sci. Technol.* **17** S213–6
- [2] Bottura L and Godeke A 2012 *Rev. Accel. Sci. Technol.* **5** 25–50
- [3] Fleiter J, Ballarino A, Bonasia A, Bordini B and Richter D 2017 *IEEE Trans. Appl. Supercond.* **27** 4004305
- [4] Yamada R et al 2007 *IEEE Trans. Appl. Supercond.* **17** 1461
- [5] Hasegawa T et al 2001 *IEEE Trans. Appl. Supercond.* **11** 3034–7
- [6] Marino I, Pujana A, Sarmiento G, Sanz S, Merino J M, Tropeano M, Sun J and Canosa T 2016 *Supercond. Sci. Technol.* **29** 024005
- [7] Kajikawa K, Uchida Y, Nakamura T, Kobayashi H, Wakuda T and Tanaka K 2013 *IEEE Trans. Appl. Supercond.* **23** 5201604
- [8] Kim S W et al 1995 *IEEE Trans. Appl. Supercond.* **5** 385
- [9] Kováč J, Šouc J, Kováč P and Hušek I 2015 *Supercond. Sci. Technol.* **28** 015013
- [10] Kopera L, Kováč P, Hušek I and Melišek T 2013 *Supercond. Sci. Technol.* **26** 125007
- [11] Kopera L, Kováč P, Kulich M, Melišek T, Rindfleisch M, Yue J and Hušek I 2017 *Supercond. Sci. Technol.* **30** 015002
- [12] Kováč P, Kopera L, Melišek T, Hain M, Kováč J, Kulich M and Hušek I 2018 *Supercond. Sci. Technol.* **31** 015015
- [13] Cubero A, Navarro R, Kováč P, Kopera P, Rindfleisch M and Martínez E 2018 *Supercond. Sci. Technol.* **31** 045009
- [14] Šouc J et al 2005 *Supercond. Sci. Technol.* **18** 592–5
- [15] Kováč J, Šouc J, Kováč P, Hušek I and Gömöry F 2013 *Physica. C* **495** 182
- [16] Brunner B, Windbichler A, Reissner M, Kováč P and Hušek I 2015 *J. Supercond. Novel Magn.* **28** 443–6
- [17] Bean C P 1964 *Rev. Mod. Phys.* **36** 31
- [18] Wilson M N 1983 *Superconducting Magnets* (Oxford: Clarendon)
- [19] Oomen P M 2000 AC loss in superconducting tapes and cables *PhD Thesis* Universiteit Twente